

We'd like to thank the Dr. S. Losa for her useful comments to further improve our manuscript. Our responses are in blue.

I propose excluding all the equations (1-7) from Part 2.2 and equation 8 from Part 4 from the text since they were already published by Pham et al. and the presented manuscript is not on the method.

As an alternative, the authors might want to move them in an Appendix.

- 1) According the reviewer's comment, we moved the text according to the equations 1-7 from Part 2 to the appendix. The corresponding text has been changed to:

“The LSEIK filter produces the correction for the model state by weighting the difference between the observations and the model state estimation. The weight coefficients are constructed by the model error covariance matrix and observation error covariance matrix. Similar as other ensemble data assimilation methods, the LSEIK filter uses the spread of sample ensemble to estimate the uncertainties of the model state. Further, a forgetting factor ρ is introduced to parameterize the imperfect model by amplifying the already existing modes of the background error (Pham et al. 1998; Pham, 2001). Furthermore, the LSEIK filter is based on an explicit low-rank approximation of the model error covariance matrix. A second-order exact sampling method is used to initialize the LSEIK filter (Pham, 2001).”

- 2) We also removed the equation 8. The texts associated with equation 9 is changed to

“... according to the observation time by $\varepsilon = 0.4 \times \exp(-0.15\Delta t)$, here Δt is the absolute time difference between observation time and DA time.”

-Lines 13 - 14: the sentence "We use ... (LSEIK) filter to characterize correlation scales in the coastal regions" could be rewritten in a way that... the authors use a Kalman-type filtering to assimilate the data..., and they use a low rank approximation of the stationary background error covariance metrics used at the analysis steps.

In revision, we changed the text to “*We use a Kalman-type filtering to assimilate the observations in the coastal regions. Further, a low rank approximation of the stationary background error covariance metrics is used at the analysis steps.*”

- Lines 230 - 232: accounting for the representation error is indeed important. Please see Janjić et al 2017 (the study also addresses the terminology issue).

Janjić, T. , Bormann, N. , Bocquet, M. , Carton, J. A., Cohn, S. E., Dance, S. L., Losa, S. N., Nichols, N. K., Potthast, R. , Waller, J. A. and Weston, P. (2017), On the representation error in data assimilation. Q.J.R. Meteorol. Soc.. . doi:10.1002/qj.3130

We added some texts to account for the measurement error and observation error in the Section 3.2:

“The error for an observation used in data assimilation mainly includes the representation error and the measurement error. The measurement error arises primarily from the measuring instruments, the temporary reading error and imperfect retrieval algorithm. According to Janjić et al. (2017), the representation error in data assimilation comprises the error due to unsolved scales or processes, the pre-processing error and the observation-operator error.”

- Lines 266 - 267: the correct references with respect to forgetting factor are Pham et al. (1998a,b) and Pham 2001.

Thank you. We updated the references to Pham et al. 1998b and Pham 2001 as suggested.

Pham, D. T., Verron, J. and L. Gourdeau, 1998a: Filtres de Kalman singuliers évolutif pour l’assimilation de données en océanographie. Compt. Rend. Acad. Sci. Terre Planètes,326, 255–260.

Pham, D. T., Verron, J. and M. C. Roubaud, 1998b: A singular evolutive extended Kalman filter for data assimilation in oceanography. J. Mar. Syst.,16, 323–340

1 **Assimilating High-resolution Sea Surface Temperature**

2 **Data Improves the Ocean Forecast Potential in the Baltic**

3 **Sea**

4 Ye Liu¹, Weiwei Fu²

5 1. Swedish Meteorological and Hydrological Institute, Norrköping 60176, Sweden.

6 2. Department of Earth System Science, University of California, Irvine, California, 92697, USA.

7

8 *Correspondence to:* Ye Liu (ye.liu@smhi.se)

9

10 **Abstract.** We assess the impact of assimilating the satellite sea surface temperature (SST) data on
11 the Baltic forecast, practically on the forecast of ocean variables related to SST. For this purpose, a
12 multivariable DA system has been developed based on a Nordic version of the Nucleus for European
13 Modelling of the Ocean (NEMO-Nordic). We use a [Kalman-type filtering to assimilate the observa-](#)
14 [tions in the coastal regions. Further, a low rank approximation of the stationary background error co-](#)
15 [variance metrics is used at the analysis steps.](#) High resolution SST from OSISAF is assimilated to
16 verify the performance of DA system. The assimilation run shows very stable improvements of the
17 model simulation as compared with both independent and dependent observations. The SST prediction
18 of NEMO-Nordic is significantly enhanced by the DA system. Temperatures are also closer to obser-
19 vation in the DA system than the model results in the water above 100 m in the Baltic Sea. In the
20 deeper layers, salinity is also slightly improved. Besides, we find that Sea level anomaly (SLA) is
21 improved with the SST assimilation. Comparison with independent tide gauge data show that overall
22 root mean square error (RMSE) is reduced by 1.8% and overall correlation coefficient is slightly in-
23 creased. Moreover, the sea ice concentration forecast is improved considerably in the Baltic proper,
24 the Gulf of Finland and the Bothnian Sea during the sea ice formation period, respectively.

25

26 **1. Introduction**

27 Monitoring the marine status of the Baltic Sea with relevant resolution and accuracy is a key
28 requirement to serve the marine policy for detecting the influence of human activities on the environ-
29 ment and better understanding the response of ocean to accelerating global climate change. The Baltic
30 Sea is one of the largest brackish seas in the world. It is a semi-enclosed basin, whose hydrography is
31 highly variable and influenced by large-scale atmospheric processes and significant influx of freshwa-
32 ter from rivers runoff and precipitation (Leppäranta and Myrberg, 2009). In addition, the water ex-
33 change between the North Sea and Baltic Sea through the Danish straits is hindered by shallow topo-
34 graphic restrictions in the transition zone (Fig. 1).

35 A characteristic feature of numerical forecast in the Baltic Sea is in itself a major challenge
36 because of complex topography and rich dynamics. A number of ocean forecasting systems for the
37 Baltic Sea have been developed using hydrological model by operational agencies around this region.
38 Traditionally, these models have a horizontal resolution of 1–5 km and approximately 20–100 layers
39 in vertical structure (Omstedt et al. 2014). Due to the geographic location and conditions of the Baltic
40 Sea, even higher resolutions are often needed to better understand the circulation dynamics. However,
41 even ocean circulation models with a particularly high spatial resolution (e.g. 1 km) cannot resolve all
42 dynamically important physical processes in the ocean (Malanotte-Rizzoli and Tziperman, 1996). In
43 general, the forecast quality for a numerical model depends on initial conditions, boundary conditions
44 (lateral, open boundaries as well as meteorological forcing and bathymetry) and a robust numerical
45 model itself. As an operational forecasting agency, the Swedish Meteorological and Hydrological In-
46 stitute's (SMHI) needs to issue well-informed forecasts and warnings for decision making by other
47 authorities during e.g. severe weather events, but also to the public. To improve the forecast quality,
48 the core three-dimensional dynamic model of the SMHI operational forecast system has recently mi-
49 grated to the Nordic version of the Nucleus for European Modelling of the Ocean (NEMO-Nordic).

50 In additional to model development, an extended observational network has been established by
51 the joint efforts of the countries surrounding the Baltic Sea. The observation platforms include vessels,
52 buoys, coastal stations, satellite, etc. Specially, the observations from satellite have dominated the

53 coverage of SST observational networks in the Baltic Sea (She et al. 2007). Among satellite products,
54 the SST is most popularly and widely used for the operational forecast, reanalysis or validation of the
55 model because of both its coverage and properties. SST acts as a medium between atmospheric and
56 oceanic variations through activation of coupling mechanisms. SST is also a key ocean variable to link
57 many processes that occur in the upper ocean, for example, air-sea exchange of energy, primary
58 productivity, and formation of water masses (Tranchant et al., 2008).

59 A realistic forecast of SST is essential to an ocean forecasting system. SST is especially im-
60 portant for the Baltic Sea that the average water depth is only 56 m and its surface water is directly
61 related to the bottom water by the mixing in the shallow sub-basins. Recently, the applications of SST
62 for forecasting and analyzing the status of the North Sea and Baltic Sea have received particular atten-
63 tion. In the short-term forecast, Losa et al. (2012, 2014) investigated the systematic model uncertain-
64 ties for forecasting the North and Baltic Seas by assimilating the Advanced Very High Resolution
65 Radiometer (AVHRR) SST data. Nowicki et al. (2015) applied SST observed from Aqua Moderate
66 Resolution Imaging Spectroradiometer (MODIS) into 3D coupled ecosystem model of the Baltic Sea
67 with the Cressman analysis scheme. O’Dea et al. (2016) enhanced the SST prediction skill of the oper-
68 ational system by assimilating both in-situ data and level 2 SST data provided by the Global Ocean
69 Data Assimilation Experiment High-Resolution SST (GHRSSST) into a European North-West shelf
70 operational model. Moreover, SST has been used in the long-term analysis in this region. For instance,
71 Stramska and Bialogrodzka (2015) analyzed spatial and temporal variability of SST in the Baltic sea
72 based on 32-years of satellite data, which indicate that there is a statistically significant trend of in-
73 creasing SST in the entire Baltic sea. However, these long-term SST data haven’t been used to verify
74 the application of sophisticated DA methods for hydrography model in the Baltic profiles simulation,
75 especially at the Baltic deep water regions. Another important question is: what amount of satellite
76 SST can improve long-term forecast of ocean variables related to SST in the Baltic Sea.

77 The objective of this study is to address the impact of assimilating a high resolution SST product
78 on the forecast of the Baltic Sea, particularly the forecast of SST related variables like sea level and
79 sea ice. It is also the first time that satellite SST from the Ocean and Sea Ice Satellite Application Fa-
80 cility (OSISAF) was assimilated into NEMO-Nordic model (NEMO variant for the North Sea and

81 Baltic Sea). For operational forecast, the SST from OSISAF is the most important dataset in the Baltic
82 Sea because it differs from hindcast analyzed product like OSTIA (Operational SST and Sea Ice Anal-
83 ysis) data. As a level 2 product, the OSISAF SST has both good temporal and spatial coverage in the
84 Baltic Sea. As there is no hindcast information included in the OSISAF SST, we are able to assess
85 direct impacts of assimilating SST observations. Therefore, exploring the potential of this product is
86 critically important to further improving the new operational forecast system. In addition, our study
87 will enrich the reanalysis database of the Baltic Sea. In this study, we use the Singular Evolutive Inter-
88 polated Kalman (SEIK) filter (Pham, 2001) to account for the model uncertainties arising from a wide
89 range of spatial and temporal scales (Haines, 2010). One of our focuses is the impact of SST on the
90 modeled sea level and the sea ice in the Baltic Sea. For the whole Baltic Sea, how the SST assimi-
91 lation influences the temperature and salinity (T/S) on the different depth is another focus of this study.

92 The outline of the paper is as follows: the model configuration and SEIK scheme are described
93 in Section 2. An overview of the observations used in this study is presented in Section 3. The imple-
94 mentation of DA experiment is given in section 4 together with the sampling of ensemble and localiza-
95 tion. Results are compared with observations for temperature, salinity, sea level anomaly and sea ice in
96 Section 5. In this section, the impact of data assimilation on the forecasts is also investigated. Conclu-
97 sions and discussions are given in section 6.

98

99 **2. Methodology**

100 **2.1 NEMO-Nordic**

101 NEMO (Nucleus for European Modelling of the Ocean; Madec, 2008) has been set up at SMHI
102 for the North Sea and the Baltic Sea, a configuration called NEMO-Nordic (Hordoir et al., 2015) (Fig.
103 1). Open boundaries are implemented in northern North Sea between Scotland and Norway and in the
104 English Channel between Brittany and Cornwall, respectively (Hordoir et al., 2013). In this study,
105 NEMO-Nordic employs a horizontal resolution of 2 nautical miles (3.7 km) and 56 vertical levels, and
106 with a vertical resolution of 3 m close to the surface, decreasing to 22 m at the bottom of the deepest
107 part of the Norwegian trench. NEMO-Nordic uses a fully nonlinear explicit free surface (Adcroft and

108 Campin, 2004). A bulk formulation is used for the surface boundary condition (Large and Yeager,
109 2004). The ocean model is coupled to the Louvain-la-Neuve Sea Ice Model (LIM3) sea ice model
110 (Vancoppenolle et al., 2008) with a constant value of 10^{-3} PSU for the sea-ice salinity. A time-splitting
111 approach is used to compute a barotropic and a baroclinic mode, as well as the interaction between
112 them. A Tidal Inversion Model is used to define the barotropic mode at the open boundary conditions
113 (Egbert and Erofeeva, 2002). 11 tidal harmonics are defined for sea level and barotropic tidal veloci-
114 ties. In addition, a coarse resolution barotropic storm surge model covering a large area of the North-
115 ern Atlantic basin provides wind-driven sea level that is added to the tidal contribution. The T/S data
116 at the open boundary are provided by the Levitus climatology (Levitus and Boyer, 1994). Radiation
117 conditions are applied to calculate baroclinic velocities at these boundaries. A quadratic friction is
118 applied with a constant bottom roughness of 3 cm, and the drag coefficient is computed for each bot-
119 tom grid cell. NEMO-Nordic uses a TVD advection scheme with a modified leapfrog approach that
120 ensures a very high degree of tracer conservation (Leclair and Madec, 2009). Unresolved vertical tur-
121 bulence is parameterized with κ - ϵ scheme (Umlauf and Burchard, 2003). In addition, Galperin pa-
122 rameterization is used to obtain a stable long-term stratification for the Baltic Sea (Galperin et al.,
123 1988).

124 A Laplacian isopycnal diffusion is used for both momentum and tracers with a diffusion parame-
125 ter that is constant in time, but varies in space. Additional strong isopycnal diffusion is used close to
126 the Neva river inflow (Gulf of St. Petersburg) in order to avoid negative salinities. The bottom bound-
127 ary layer is parameterized to ease the propagation of saltwater inflows between the Danish Straits and
128 the deepest layers of the Baltic Sea (Beckmann and Doscher, 1997). A free-slip option is used for lat-
129 eral boundaries.

130 The model is forced by meteorological forcing derived from a downscaled run of Euro4M reanaly-
131 sis (Dahlgren et al., 2014). The downscaling is based on the regional atmospheric model RCA4 (Sam-
132 uelsson et al., 2011) which uses the reanalysis data as boundary conditions. A runoff database provides
133 the river flow to NEMO-Nordic (Donnelly et al. 2016); it includes inter-annual variability for the Bal-
134 tic Sea basin and is based on climatological values for the North Sea basin. The salinity of the river
135 runoff is set to a constant value of 10^{-3} PSU, which is the same value used for the sea-ice to avoid any

136 negative salinity.

137

138 **2.2 Local Singular Evolutive Interpolated Kalman (LSEIK) filter**

139 The method used to assimilate SST into NEMO-Nordic is the Local Singular Evolutive Interpo-
140 lated Kalman (LSEIK) filter (Pham et al., 2001, Nerger et al. 2006). This is a sequential data assimila-
141 tion scheme, which is an error subspace extend Kalman filter that uses a minimum number of ensem-
142 ble members to reduce the prohibitive computation burden (Pham, 2001). The LSEIK filter produces
143 the correction for the model state by weighting the difference between the observations and the model
144 state estimation. The weight coefficients are constructed by the model error covariance matrix and
145 observation error covariance matrix. Similar as other ensemble-based data assimilation methods, the
146 LSEIK filter uses the spread of sample ensemble to estimate the uncertainties of the model state. Fur-
147 ther, a forgetting factor ρ is introduced to parameterize the imperfect model by amplifying the already
148 existing modes of the background error (Pham et al. 1998; Pham, 2001). Furthermore, the LSEIK filter
149 is based on an explicit low-rank approximation of the model error covariance matrix. A second-order
150 exact sampling method is used to initialize the LSEIK filter (Pham, 2001). Localization was also used
151 to remove the unrealistic long-range correlation with a quasi-Gaussian function and a uniform hori-
152 zontal correlation scale (Liu et al. 2013). It was performed by neglecting observations that were be-
153 yond correlation distance from an analyzed grid point. In other words, only data located in the “neigh-
154 borhood” of an analyzed grid point should contribute to the analysis at this point (Liu et al. 2009; Jan-
155 jić et al. 2011).

156

157 **3. Observations**

158 **3.1 Satellite observations**

159 The satellite SST used in DA was provided by OSISAF (<http://osisaf.met.no/p/sst/index.html>).
160 OSISAF aim is to produce, control and distribute operationally in near real-time products using avail-
161 able satellite data. The satellite datasets product used here includes the observations from polar orbit-
162 ing satellites (the EUMETSAT MetOp-A and NOAA-18, -19) with the AVHRR instrument. The SST

163 product has a resolution of 5 km and is produced twice daily at 00 UTC and 12 UTC. It covers the
164 Atlantic Ocean from 50°N to 90°N. The SST observations are thermal infrared observations from the
165 AVHRR instrument and are therefore limited by cloud cover (Kilpatrick et al. 2001). The cloud mask
166 in use is based on a multi-spectral thresholding algorithm by SMHI. The products were retrieved using
167 a nonlinear split window algorithm (Walton et al. 1998). The coefficients in the retrieval algorithm are
168 determined through regression toward in situ observations, and the dataset thus represents the subskin
169 temperature of the oceans. Further, subskin observations are subject to diurnal warming effects, which
170 can be significant in the Baltic Sea. Here only the subskin SST at night (00 UTC), which is compara-
171 ble to in situ (buoy) measurement, is used to minimum this effect. The SST is controlled with the cli-
172 matology check. A quality level from 0 to 5 is associated with every pixel. The higher level value, the
173 better the quality of the observations (Brisson et al., 2001). Observations with quality level 4 (good) or
174 5 (excellent) are collected for the analysis and low quality observations were removed. By applying
175 the above quality control processes, only a subset of the original OSISAF products is kept in this
176 study. Based on the former validation, a bias value of 0.5°C is given for this product.

177 Further, the IceMap from a sea ice concentration dataset with a high spatial resolution of 5 km
178 (http://www.smhi.se/oceanografi/iceservice/is_prod_en.php) is used to validate the DA results. It is
179 produced by SMHI and originates from digitized ice charts. An advantage of this data is that the ice
180 charts are quality checked manually. However, the drawback is that they include some subjective
181 steps. The temporal resolution of the IceMap SST is twice a week in the experiment period. Sea ice
182 occurs most frequently in the Bay of Bothnia, with up to 100 ice covered days per year. However, sea
183 ice can occur in all parts of the Baltic Sea and Danish straits, demonstrating the need for careful treat-
184 ment of sea ice in the SST analysis.

185

186 **3.2 In situ data**

187 The observations from the German Maritime and Hydrographic Agency (BSH) moored buoy
188 stations were collected as independent dataset to validate the assimilation results. The observations
189 have high temporal resolution and long continuous record. The second dataset was downloaded from
190 the Swedish Oceanographic Data Centre -SHARK database (<http://sharkweb.smhi.se>). SHARK mainly

191 contains low-resolution CTD data from a list of predefined standard stations in the Baltic Sea, as well
192 as in Kattegat and Skagerrak. Only observations that have passed gross quality control procedures are
193 collected into the SHARK database. This procedure includes, for example, location checks and local
194 stability checks. In addition, validating data records from tide gauges are also used. The sea level
195 anomaly measurements from tide gauges (sea level stations) are measured in a local height system and
196 values are presented relative to theoretical mean sea level, a level calculated from many years of annu-
197 al means, which takes into account the effect of land uplift and sea level rise. The values are averaged
198 over one hour period.

199 Not all the available observations from satellite, moored buoys, CTDs, tide gauges were included
200 in this study. To obtain the high assimilation quality results, another quality control was applied for
201 these data before they were used into assimilation and validation. These controls include examination
202 of forecast observation differences by excluding those observations for which the difference between
203 the forecast and the measurement exceeded given standard maximum deviations. The criteria were set
204 up empirically based on past validation results of the model (Liu et al. 2013). Furthermore, stations
205 located on land, according to the NEMO-Nordic grid, were excluded. We also removed the duplicate
206 records of these data.

207 The accuracy of observation error is difficult to be defined for all water points. The observation
208 is commonly assumed to be spatially irrelevant, which results in an error covariance matrix that is
209 time-invariant diagonal and its diagonal elements equal the variance of observation error. [The error for
210 an observation used in data assimilation mainly includes the representation error and the measurement
211 error. The measurement error arises primarily from the measurement device alone, the temporary read-
212 ing error and imperfect retrieval algorithm. According to Janjić et al. \(2017\), the representation error
213 in data assimilation comprises the error due to unsolved scales or processes, the pre-processing error
214 and the observation-operator error.](#) In this study, the observation error was estimated to one value as
215 the sum of all observation uncertainties used in the analysis. Besides, the uncertainties of satellite SST
216 varies from coast to the open sea, i.e. higher uncertainties in the coast region relative to the open sea.
217 We used a constant standard deviation value of 0.4°C based on the standard deviation of satellite SST,
218 which ranged from the ~0.1°C to ~0.5°C in the Baltic Sea (She et al. 2007, Høyer et al. 2016).

219

220 **4. Configuration of LSEIK in the experiment**

221 As above mentioned, the initialization of the filter requires an initial analyzed state and a low
222 rank approximation of the corresponding estimation of error covariance matrix. The data assimilation
223 process was initialized by a free model simulation. First the model was spinning up 20 years to reach a
224 statistically steady state. Then a further (free-run) integration covered the period 2006-2009 was car-
225 ried out to generate a historical sequence of model state. To reduce the calculation cost, we took a
226 snapshot in every 6 days and saved 183 state vectors, which includes sea level, temperature and salini-
227 ty, in total to describe the model variability because successive states are quite similar. The initial en-
228 semble provided an estimate of the initial model state and its uncertainty before the assimilation of
229 SST observations. The quantity of the model variability was expected to be reasonably comparable
230 with the forecast error, which was dominated by misplacement of mesoscale features and varies in
231 location and intensity seasonally. Further, the very high frequencies of model variability were also
232 unfavourable in an ensemble of state vectors for SST data assimilation (Oke et al., 2005). Therefore, a
233 band-pass filter was used to remove the unwanted frequency of model variability. To initial low rank
234 error covariance matrix, a multivariable Empirical Orthogonal Functions (EOF) analysis was applied
235 on the 183 state vectors of model variables (sea level, temperature and salinity). In the North Sea and
236 Baltic Sea, error covariances of different variables are not uniform and strongly dependent on whether
237 the variable resides in the open sea or coastal zone. Each state variable was then normalized by the
238 inverse of its spatially averaged variance at every model level. At last, 34 leading EOF modes were
239 kept and they explained 85% overall variability. Then the initial error covariance matrix was estimated
240 by $P^a(t_0) \approx L_0 U_0 L_0^T$, where the L_0 is composited by the leading EOF modes and U_0 is diagonal
241 matrix with the corresponding eigenvalues on its diagonal. We used a time-invariant sample ensemble
242 to approximate the background error covariance during the experimental period (Korres et al, 2004;
243 Liu et al. 2017). This stationary ensemble affords a good approximation of the ocean's background
244 error covariance. Meanwhile, it is computationally efficient for our objective.

245 The localization scale is another import factor to the assimilation system, especially at the coastal

246 region. Large correlation scale may transfer artificial increments to the positions far away from the
247 analysis observation during the DA process. However, small correlation scale is prone to cause the
248 singularity of ocean state around analyzed observation and break the continuity of the ocean state.
249 Hence, an unreasonable scale causes the instability of the model integration or degrades the assimila-
250 tion quality. Unfortunately, the accuracy length for the correlation is unknown for the North Sea and
251 Baltic Sea. The correlation length scale is to some extent dependent on the Rossby radius of defor-
252 mation (Losa et al., 2012), which varies from ~ 200 km in the barotropic mode to ~ 10 km or even less
253 in the baroclinic mode (Fennel et al., 1991; Alenius et al, 2003). According to the former researches
254 like Liu et al. (2013, 2017), a length scale of 70 km was specified for both the North Sea and Baltic
255 Sea in this study. Not that this value may be not perfect and more accurate correlation length needs to
256 be tested for LSEIK. For example, spatially variable length scales are the next step for the regional DA
257 simulations.

258 To define the forgetting factor, a one-month simulation experiment with varying the factor ρ was
259 done in January 2010. At last, a factor $\rho = 0.3$ resulted in the best assimilation performance. Further,
260 we define a two-day assimilation window in assimilation experiment. As a result, the observations in
261 the two days before the assimilation time were used to calculate the innovation with observation oper-
262 ator. When we calculated the innovation we also changed the observation error according to the obser-
263 vation time by $\varepsilon = 0.4 \times \exp(-0.15\Delta t)$, here Δt is the absolute time difference between observation
264 time and DA time.

265

266 **5. Results**

267 In the following sub-sections, we conducted two runs with and without assimilation of the
268 SST observations from the OSISAF database, both runs with the above setup of the analysis system.
269 Accordingly, the runs with and without assimilation are called ASSIM and FREE, respectively. We
270 considered the evolution of SST based on 48-hourly local analysis from 1 January 2010 to 31 Decem-
271 ber 2010. The 48-hourly forecast SST from two runs was assessed with observations from different
272 dataset. Then we analyzed the impact of the data assimilation on the profile simulation of T/S. At last,

273 we evaluated the system performance with respect to sea surface anomaly and sea ice, respectively.

274

275 **5.1 Comparison with satellite data**

276 First, we presented two cases to show the ocean state before and after the assimilation of the
277 OSISAF SST data in Fig. 2. The first case was given at 11 January 2010, a date with clear weather and
278 many observations available. The model has obvious difficulties in reproducing the observed SST.
279 The cold biases in the forecast were found in the Skagerrak, west coast of the Baltic proper and the
280 Bothnian Bay, respectively. However, the warm biases appeared in the interior of the Baltic Sea and
281 the Kattegat. The largest deviation in the FREE reached 2.2 °C at the Skagerrak. Apparently, tempera-
282 ture by assimilation analysis agreed with the satellite-derived data much better. This correction at the
283 analysis step has allowed us to reduce the deviation of the SST forecast from the observations. The
284 DA system simulation was also verified at 2 June 2010, which has also many available OSISAF ob-
285 servations. The biases on 2 June 2010 were obviously different from that on 11 January 2010. Moreo-
286 ver, it was found they had a roughly opposite bias signal. For example, relative to the OSISAF SST at
287 the Baltic proper, Bothnian Sea and Bothnian Bay, FREE produced relatively warmer water at January
288 11 and colder water at 2 June (Fig. 2), respectively. After data assimilation, the analysis increments
289 were appropriately added to the model field. In general, the SST DA has improved the simulated SST
290 in both cases (Fig. 2).

291 Maps of annual averaged RMSE of SST from two runs relative to the IceMap observation are
292 shown in Fig. 3. Obviously, the RMSE in FREE and ASSIM had different distribution in the Baltic
293 Sea. In general, FREE had smaller error in the Skagerrak, eastern the Kattegat and the interior of the
294 Bothnian Sea relative to other subbasin of the Baltic Sea. The largest RMSE was found at the connec-
295 tion region between the Baltic proper and the Bothnian Sea. This could be caused by the shallow wa-
296 ter, complicated bathymetry and large observation biases in this area. It was also noted that the RMSE
297 was larger in the coast region compared to its interior in the Baltic proper and Bothnian Sea. After the
298 assimilation, the SST has been significantly improved. The RMSE of SST from ASSIM was generally
299 smaller than 1.0 °C. However, there were still some regions where the improvements were relatively
300 small and the RMSE of SST was greater than 1.0 °C. These large errors were predominantly located at

301 the edge of the Baltic Sea and the Danish straits. For instance, the RMSE of SST was greater than 1.2
302 °C at both the entrance of the Gulf of Finland and the west coast of the Bothnian Sea. The relatively
303 small improvements were regularly caused by the rare observations or the less accurate observations
304 near the coast water.

305 The overall daily averaged SST errors against the IceMap observations have been estimated
306 (Fig. 4). The observations had better coverage in summer and autumn than in winter and spring. The
307 variability of the number of observation directly affected the assessment of DA results. The model
308 biases had pronounced seasonal variability, which had small values in spring and winter. In general,
309 the assimilation provided better SST estimations. The free run had a RMSE of 1.47 °C. After the as-
310 simulation, the RMSE was reduced to 1.03 °C, whereas the bias was reduced by 0.73 °C. An interesting
311 feature was that the SST error reduction due to the assimilation was almost consistent with the varia-
312 bility of the number of IceMap observations. For example, the improvement became large with in-
313 creasing the number of IceMap observations from March to June 2010. However, the number of ob-
314 servations was kept constant during the period June-November 2010 and the improvement shown in
315 both the bias and RMSE of SST did not exhibit large variability, which meant reliable performance of
316 the DA system.

317

318 **5.2 Comparison with independent in-situ data**

319 The time series of T/S were compared with independent observations located at Arkona station
320 (13.87°E, 54.88°N) in the Arkona Basin and at BY15 (20.05 °E, 57.33 °N) in the Eastern Gotland Ba-
321 sin, respectively. These two stations were selected to verify the experiment results because of their
322 relatively completed observation records for the experiment period. In the Arkona Basin, the water
323 depth was shallow and the water column can be well mixed between surface and bottom water. Thus,
324 the bottom T/S was largely affected by the surface dynamic (Liu et al. 2014). Relative to observations,
325 the model had warm biases at this station (Fig. 5). At a depth of 25m, the observed temperature
326 showed the largest variability, which was a good representation of the bottom characteristics of the
327 mixed layer. In mid-August, the temperature was abruptly increased by 10°C at a depth of 25m and
328 slightly decreased at surface, respectively. The reason is that the surface water suddenly sinks to deep-

329 er layers, which warm the deep water. However, this dynamic process hasn't reached to Arkona bot-
330 tom and it didn't cause the obvious bottom temperature variability (Fig. 9). Both FREE and ASSIM
331 had reproduced this process, whereas FREE showed larger temperature biases. To the salinity at the
332 Arkona station, the surface observations were missing, the comparison at 7 m depth verified the sub-
333 surface simulations. The observations showed larger salinity variability in winter relative to summer.
334 This pronounced seasonal variation is associated with the variation of fresh river runoff and net E-P
335 (Evaporation-Precipitation) flux (Fu et al, 2012). At a depth of 7 m, salinity was obviously underesti-
336 mated from April to September and overestimated after November although the ASSIM had slightly
337 better results compared to FREE. The DA also provided better simulation of salinity at 25 m depth.
338 For example, the salinity bias in the October was reduced by 3 psu by DA. At a depth of 40 m, the
339 saltwater inflows were observed, resulting in sudden increases of salinity. For instance, the salinity
340 was increased by 3.5 psu in February followed by a decreasing trend. The variations were reproduced
341 in both FREE and ASSIM, whereas the intensity of the decreased process is weakly simulated with a
342 difference of 3 psu and the inflow in March was not strong enough relative to the observed one. Ob-
343 servations also showed a large salinity variability amounts to 4–8 psu in the autumn. Although FREE
344 and ASSIM had shown these changes, their magnitude was obvious weaker than observations. The
345 possible reason was that the model's resolution was inadequate to well resolve the topography and
346 eddies in this area. Both the large runoff and the complicated bathymetry posed challenges for the
347 model to tackle the small-scale dynamic process in such a shallow basin. A higher resolution model
348 perhaps was more preferable to study this dynamic process.

349 The Eastern Gotland Basin has deeper water depth compared to the Arkoan Basin, in which the
350 water column is permanently stratified and the halocline lies at about 60–80 m (Fu et al, 2012). The
351 mixing and sinking of T/S are hindered by the strong stratification. Unlike observations in the Arkona
352 Basin (Fig. 5), the CTD observations at BY15 had lower temporal resolution with almost one observa-
353 tion per month. In the mixing layer, it can be seen model had overestimated the temperature (Fig. 6).
354 At a depth of 10 m, ASSIM has remarkably improved the simulation of temperature relative to FREE.
355 The bias has been reduced by 3°C in the spring of 2010. At 175 m depth, observed temperature
356 showed very small variation. The reason was that the main source for deep water ventilation is the

357 saltwater inflows which are suppressed by runoff within a depth range of 75–135 m in the Eastern
358 Gotland Basin (Vali et al. 2013). As a result, updating the bottom water is very slow. Both FREE and
359 ASSIM overestimated the temperature in the spring and the beginning of summer of 2010. Further,
360 ASSIM has increased the temperature bias after mid-summer relative to FREE. This result might be
361 explained by that the strong correlation isn't expected between surface and layers below the halocline
362 because of the strong stratification in this basin, which perhaps yield the artificial correction. There-
363 fore, the improvement of the surface temperature cannot guarantee its positive influence on the bottom
364 temperature. To the salinity, the model had less accurate simulation with generally low salinity biases
365 at 10 m depth. ASSIM provided better salinity simulation compared to FREE. At 70 m depth, the
366 small variation of salinity was found after DA. Moreover, at 175 m depth, the observation had very
367 small variability about 0.1 psu. In general, both experiments have reproduced these variations. How-
368 ever, FREE increased salinity by 0.2 psu from March to April relative to the observation, which
369 caused the overall salinity overestimated amount to 0.2 psu. This increasing process wasn't shown in
370 observations and the reason remained unclear. The DA has shown slight improvement, but it still salt-
371 er than the observations.

372 The mixed layer depth (MLD) was calculated at the Arkona and BY15 station and compared with
373 the SHARK observation in Fig. 7. We used the temperature criterion to define the MLD, i.e., the depth
374 at which the temperature deviated from the surface value by 0.5 °C (Fu et al., 2012). Figure 7 shows
375 that the MLD at Arkona had larger variability relative to the MLD at BY15. The reason contributed to
376 this feature is that the deeper water at Arkona is easy affected by wind forcing because of the shallow
377 bathymetry and well mixing, whereas the temperature variation in upper water at BY15 difficulty in-
378 fluences the deeper water because of the strong stratification. Both runs had reproduced the MLD var-
379 iability feature similar as the observations. For example, the minimum MLD appeared in summer,
380 which was about several meters. The assimilation of satellite SST caused strong changes in the MLD
381 at both stations, especially in winter. One explanation was that the Baltic Sea was largely affected by
382 wind forcing and the winter wind was much stronger than the summer wind. Further, strong heating in
383 summer promoted stratification in summer and shoaled the MLD.

384 Further, the temporal and spatial distribution of the SHARK observations is shown in Fig.8.

385 These observations were unevenly distributed in the Baltic Sea. In the Skagerrak, the observations
386 appeared at the Danish and Swedish coast. However, in the Bornholm Basin, Kattegat, and Baltic
387 proper, the observations mainly were found in the central and the Swedish coast side. There were also
388 many observations in the Bothnian Sea and rare observations in the central of the Bothnian Bay. It
389 must be noticed that there aren't SHARK observations in both the Gulf of Finland and Gulf of Riga
390 during the experiment period. Moreover, these SHARK profiles in the first four months were mainly
391 located from the Skagerrak to the Baltic proper, which are relatively rare in the northern Baltic Sea. In
392 the Bothnian Bay, the observations are mainly in the winter period.

393 Figure 9 shows the change of overall bias and RMSE of T/S with depth against the SHARK
394 dataset. In the Baltic Sea, DA had large impact on the temperature forecast in the water above 100 m.
395 The RMSE showed that the forecast of temperature was obviously improved from surface to thermo-
396 cline in the ASSIM and the improvements generally decreased with depth. Above 100 m, the overall
397 RMSE of temperature in ASSIM was decreased by 21.38% (from 1.59 to 1.25 °C). It was also found
398 the temperature error had similar variability as the warm biases in two runs. In the transition zone, the
399 RMSE in the ASSIM was reduced by 5.59% and -20.31% above and below 100 m relative to the
400 FREE, respectively. Below 90 m, the temperature was also over-adjusted, which changed the warm
401 bias to cold bias. It is worth noting that the number of the deeper water observation in the transition
402 zone is substantially less than that in the Baltic Sea. For the salinity, both RMSE and bias of the AS-
403 SIM showed very minor changes relative to the FREE inside the Baltic Sea. For the water above 100
404 m, the total RMSE of salinity was increased by 3.48% (from 1.15 psu in the FREE to 1.19 psu in the
405 ASSIM) in the transition zone and 1.04% (from 0.96 psu in the FREE to 0.97 psu in the ASSIM) in
406 the Baltic Sea.

407

408 **5.3 Sea Level Anomaly**

409 SLA represents a vertically integrated effect of the T/S variations over the whole water col-
410 umn. The accurate simulation of SLA is thus a good indicator of the model performance. Therefore,
411 validating the impact of SST assimilation on the simulation of SLA is very important to the Baltic Sea
412 forecast. The observations from the 24 tide gauge stations were used. These gauge stations are mainly

413 located at the Swedish coast (see Fig.8b). Since only the SST is assimilated in this study, the SLA
414 observations are completely independent.

415 We calculated the RMSE and correlation coefficients for both the FREE and ASSIM against the
416 observations from tide gauges (Fig. 10). The overall RMSE was reduced by 1.8% and the correlation
417 coefficients were slightly increased. Among these stations, RMSE at the Oskarshamn was decreased
418 by 5.6%, which is larger than that in other station. The minimum RMSE change of SLA was seen at
419 the Klagshamn. For the correlation coefficient, improvement on the SLA by the DA is very small.
420 Simrishamn station showed the biggest change of correlation coefficient, which is 1.1%. The RMSE
421 and correlation comparison demonstrated that the SST DA has generally positive effects on the fore-
422 cast of the SLA.

423 In addition, the time series of the SLA error discrepancy (ASSIM minus FREE) in two runs at
424 four stations were selected to evaluate the simulation results (Fig. 11). These four stations were select-
425 ed to represent the model performance at different positions of the Swedish coast. Two runs showed
426 evidently different performance in these four stations. The variability of the SLA difference between
427 two experiments at the Smogen station had higher frequency compared to other stations. The reason
428 was that the Smogen station was located at the transition zone where the water had higher frequency
429 variations caused by the brackish Baltic in/outflowing relative to other three stations. At these four
430 stations, the improvements were mainly in later spring and summer, whilst the degraded simulations
431 were mostly happened after Mid-September, respectively. The SST assimilation had less impact in late
432 winter and early spring compared to other seasons. Besides, the impact of SST assimilation on SLA
433 simulation was not same in the four positions. For instance, during the period from Mid-November to
434 Mid-December, the SLA in ASSIM was improved at Simrishamn and degraded at both the Ratan and
435 LandsortNorra stations, respectively. This phenomenon was possibly caused by the imperfect correla-
436 tion between SST and SLA in the stationary samples. Further, these steric small changes of SLA by
437 DA were what we expected because only SST was assimilated into Nemo-Nordic.

438

439 **5.4 Sea ice**

440 Sea ice in the Baltic Sea occurs primarily in its north region and influences the Baltic climate.

441 Accurate detecting the sea ice is very useful to the northern Baltic living because too much or too little
442 sea ice can be a problem for wildlife and people. Sea ice concentration (SIC) and Sea ice extent (SIE)
443 are two important and common indicator to modeling sea ice environment. We assessed the SIC and
444 SIE from simulations against the IceMap observations in Fig. 12-13. Differ from the daily evaluation
445 in Losa et al. (2014), the monthly mean SIC was used to represent the general status of sea ice in the
446 Baltic Sea. Besides, SIC in January, February and December showed the variation of the sea ice in
447 winter.

448 In January 2010, the observations showed large ice coverage in the Bothnian Bay and the Gulf
449 of Finland and small SIC in the Gulf of Riga, respectively. Model generally reproduced this distribu-
450 tion of sea ice. However, FREE simulated too much sea ice in the Gulf of Finland and the eastern
451 coast of the Baltic proper relative to observations. For example, SIC from FREE almost to 30% higher
452 than observations along the Estonia coastline. It could be seen that the SST DA reduced these biases.
453 The reason is the SST DA modified the thermal expansion by providing the well temperature fields
454 above the thermocline. The temperature in February became colder relative to January in the Baltic
455 Sea. As a result, the sea ice in February extended to the Bothnian Sea and the whole Gulf of Riga.
456 Observation also showed small SIC in Kattegat and Skagerrak. Model simulated higher SIC in the
457 Bothnian Sea with largest biases along the Swedish and Finnish coast. As an example, the observed
458 ice in the Bothnian Sea was characterized by concentrations mainly smaller than 0.5, whereas modeled
459 ice in FREE had concentration greater than 0.9 in the shallow region of the Bothnian Sea. FREE also
460 had smaller ice coverage with lower SIC in the transition zone between the North Sea and the Baltic
461 Sea relative to IceMap. After the SST assimilation, ASSIM reduced SIC in the Bothnian Bay and the
462 west coast of the Baltic Sea, which was closer to the observations. The ice in ASSIM didn't have ob-
463 vious variation in Kattegat and Skagerrak yet. ASSIM also reduced too much ice at the southern of the
464 Bothhomn Basin. The reason is that the satellite SST observations had limited accuracy near the coast
465 and they could bring artificial information into the modeling. In March, compared to observation, the
466 FREE produced low SIC in the western coast of the Bothnian Sea, Gulf of Finland, Gulf of Riga and
467 the connect zone between the Bothnian Sea and Gulf of Finland. However, the model SIC in the FREE
468 was higher than IceMap in the interior the Bothnian Bay. For instance, the SIC from FREE in the

469 western Bothnian Sea was 40% higher than observation. In the south coast of the Arkona basin and
470 Baltic proper, the FREE failed to reproduce the sea ice as in observation. After the DA, the high SIC
471 was decreased in western Bothnian Sea and closer to that in IceMap in Bothnian Sea. In the Gulf of
472 Finland and Gulf of Riga, the SIC error was increased in the ASSIM. In April, the large SIC error in
473 the FREE was shown in the Bothnian Sea, the Bothnian Bay, Gulf of Riga and Gulf of Finland, where
474 no clear improvements were seen in the ASSIM. In December, sea ice coverage was smaller because
475 of relatively warm temperature compared to that in other winter month. Most of the sea ice with high
476 concentration was observed at the edge of the Bothnian bay. Nevertheless, high concentration ice in
477 FREE also happened at the transition zone between the Bothnian Sea and Bothnian bay. Relatively,
478 ASSIM reduced the high concentration biases of sea ice. By contrast, both ASSIM and FREE had
479 lower concentration ice than observation in the eastern coast of the Bothnian Sea. The SIC from AS-
480 SIM was relatively lower than that from FREE in the northern Finish coast, whereas the observations
481 had high concentration ice there.

482 The daily SIE from FREE and ASSIM was compared with observations in Fig.13. The observed
483 SIE was generally increased from January to February and reached the maximum in mid-February.
484 During the period of March-May, SIE was decreased as temperature was increasing. SIEs in both the
485 FREE and ASSIM experiments were generally underestimated by comparison with the observation in
486 2010, especially in the period from Mid-March to early April. The SIE bias in both runs was roughly
487 increased from January to early April. In early April, the maximum negative bias of SIE was found to
488 be 105000 km² for ASSIM and 10000 km² for FREE. The impact of SST assimilation on the SIE was
489 positive during the phase of sea ice formation. For example, the SIE bias was reduced 25000 km² at
490 end of February and in the Mid-December. However, during the phase of sea ice melting (March to
491 April), the SIE error was increased in ASSIM even with the error of SST decreased. For example, the
492 SIE bias in ASSIM was increased by 42000 km² relative to FREE in the early March. These increased
493 SIE error in March mainly happened in the Gulf of Riga and Gulf of Finland (Fig.11).

494

495 **6. Conclusion and discussions**

496 A DA system based on a LSEIK filter has been coupled to the NEMO circulation model of the
497 North and Baltic Seas. The method was successfully applied for assimilating high resolution satellite
498 SST data. We demonstrated that, over the period of 2010, the agreement of the SST forecast with the
499 independent satellite observation was improved by $\sim 29.93\%$ in comparison with the regular forecast
500 without DA. The assimilation quality is directly related to the number of observation.

501 Compared with independent in-situ data from SHARK, the RMSE of temperature was reduced
502 by 21.38% and 5.59% for the water above 100 m inside and outside of the Baltic Sea, respectively.
503 However, in the deeper layers, the temperature was slightly degraded in the Baltic Sea. This is partial-
504 ly caused by the artificial correlation between surface layer and deeper layers. The improvement of
505 temperature by SST DA can't guarantee corresponding improvement of the salinity. The statistics
506 displays the salinity RMSE was increased by 1.04% and 3.48% in the transition zone and the Baltic
507 Sea, respectively. Both ASSIM and FREE have captured the main dynamic process in the Baltic Sea,
508 for example, the inflow and the sink. However, ASSIM is closer to the observed one relative to
509 FREE.

510 The forecast results were further validated with the independent SLA observations. The result
511 shows that all RMSEs and correlations for all 21 stations are smaller than 0.12 m and greater than
512 0.86, respectively. After DA, the SLAs at these stations have been slightly improved. In general, the
513 RMSE was reduced by 1.8% and correlation coefficients were slightly increased, respectively. Fur-
514 ther, the model-observation comparison at selected four stations indicates that these improvements are
515 mainly in later of spring and summer. The comparisons also denote the SST assimilation has less im-
516 pact in the late winter and early spring relative to other seasons.

517 When compared with monthly mean observations of SIC, both assimilation run and free run
518 reproduced main spatial distributions of sea ice in the Baltic Sea. During the sea ice formation period,
519 the SST assimilation has improved the results of SIC from FREE in the Gulf of Finland, the Bothnian
520 Sea and eastern coast of the Baltic proper. However, minor improvements were found in Kattegat and
521 Skagerrak. Besides, over the sea ice melting period, the SIE comparison showed the SST assimilation
522 increased the SIE error, especially in the Gulf of Finland and Gulf of Riga.

523 The daily MLD from two runs has been compared with the observations at Arkona and BY15

524 stations. Model could capture the variability features of the MLD. Similar as Fu et al.(2012), it was
525 found that SST assimilation had less impact on the MLD in summer than that in winter. In general, the
526 SST DA produced less influences on the MLD in the deeper region (BY15) relative to that in the shal-
527 low region (Arkona).

528 Further, the reliability of the DA system is worth being assessed. In Rodwell et al.(2006), a per-
529 fect reliable system error variance for ensemble assimilation was calculated by the sum of the variance
530 of the sample ensemble, the square of innovation(misfit between observation and model) and the vari-
531 ance of observation at assimilation time. In this study, we used a constant observation error similar to
532 Rodwell et al. (2016) because our DA design is different from that paper. The major difference be-
533 tween these two studies is that we estimate the background error covariance from stationary ensemble
534 and avoid the perturbation of observation error. Therefore, the variance of the sample ensemble and
535 observation is univariate and the diagnostic of the assimilation stability can be directly obtained from
536 the forecast error like the RMSE in Fig.4.

537 The results of the SST assimilation are encouraging and the assimilation helps to ameliorate
538 some model deficiencies such as the simulation of sea ice in the Gulf of Finland. However, some prob-
539 lems need to be further addressed in the SST DA in the future: firstly, the SST assimilation has worse
540 influence on the simulation of salinity in the upper layers and temperature in the deeper layers. Losa et
541 al.(2012) denoted that the salinity simulation quality crucially depends on the assumptions about the
542 model and data error statistics. Here a stationary ensemble sample was used to represent the correla-
543 tion between T/S and between surface and deep water. These relationships could be changed with the
544 varying dynamics and forcing conditions. More sophisticated assumption should be used in the DA of
545 Baltic Sea. Secondly, the SHARK observations in this study are absent at the Gulf of Finland and Gulf
546 of Riga. This denotes the validation results with SHARK observation didn't include the evaluation of
547 the simulation of T/S in deep water of these two basins. Thirdly, the univariate localization scale used
548 in this study could be another problem. The spreading of observation information strongly depended
549 on the correlation scale. The large localization scale can introduce the artificial information, which
550 could degrade the assimilation quality. A flow-dependent background error covariance with varying
551 correlation scale may be more appropriate for the Baltic Sea with complex bathymetry and rich dy-

552 namics. Fourthly, the remote sensing observations near the coast could have large bias because of the
 553 limit of the instrument itself. More strict quality controlling method needed to be used for the satellite
 554 coastal observations before their assimilation.

555
 556 Appendix

557 Here, we describe the details of the mathematical formulation used in the forecast and correction
 558 (analysis) steps of the LSEIK filter:

559 1. Forecast: the analysis state \mathbf{X}^a at time t_{i-1} is integrated forward to the time of the next available
 560 observations t_i to compute the forecast state \mathbf{X}^f ,

$$\mathbf{X}^f(t_i) = \mathbf{M}(t_{i-1}, t_i)\mathbf{X}^a(t_{i-1}) \quad (1),$$

562 where \mathbf{M} denotes the nonlinear dynamic model operator that integrates a model state from time t_{i-1}
 563 to time t_i . The superscript ' f ' and ' a ' denote the forecast and analysis. The corresponding error covar-
 564 iance matrix can be expressed as:

$$\mathbf{P}^f(t_i) = \mathbf{L}_i[(r + 1)\mathbf{T}^T\mathbf{T}]^{-1}\mathbf{L}_i^T + \mathbf{Q}_i \quad (2),$$

$$\mathbf{L}_i = \mathbf{X}^f(t_i)\mathbf{T} \quad (3),$$

567 with \mathbf{Q}_i being the covariance matrix of model uncertainties and $r + 1$ is the minimum number of
 568 sample ensemble members for error covariance matrix. The superscript ' T ' denotes the transpose of
 569 matrix. The full rank matrix \mathbf{T} has a dimension of $(r + 1) \times r$ with zero column sums and \mathbf{L} is a full
 570 rank $(r + 1) \times r$ matrix which implicitly represents the model variability.

571 2. Correction: when the observation is available at time t_i , the LSEIK filter merged the information
 572 from model and observation to produce the analysis state with the formula:

$$\mathbf{X}^a(t_i) = \mathbf{X}^f(t_i) + \mathbf{K}_i[\mathbf{Y}^o(t_i) - \mathbf{H}_i\mathbf{X}^f(t_i)] \quad (4),$$

574 Here \mathbf{Y}^o is a vector of observations. The gain matrix \mathbf{K} , which linearly interpolates between the obser-
 575 vations and the forecast, is given by

$$\mathbf{K}_i = \mathbf{P}_i^f \mathbf{H}_i^T (\mathbf{H}_i \mathbf{P}_i^f \mathbf{H}_i^T + \mathbf{R}_i)^{-1} = \mathbf{L}_i \mathbf{U}_i (\mathbf{H}_i \mathbf{L}_i)^T \mathbf{R}_i^{-1} \quad (5),$$

577 where \mathbf{H}_i denotes the linearization of observation operator, which mapping the model space to the

578 observation space. \mathbf{R} is the observation error covariance matrix. The matrix \mathbf{U}_i is updated according to

579
$$\mathbf{U}_i^{-1} = \rho(r + 1)\mathbf{T}^T\mathbf{T} + \mathbf{L}_i^T\mathbf{H}_i^T\mathbf{R}_i^{-1}\mathbf{H}_i\mathbf{L}_i \quad (6).$$

580 Here ρ is A forgetting factor.

581 A second-order exact sampling is used to initialize the LSEIK filter. At time t_{i-1} , a analysis
582 state $\mathbf{X}^a(t_{i-1})$ and its corresponding error covariance matrix $\mathbf{P}^a(t_{i-1})$, in the factorized form

583 $\mathbf{L}_{i-1}\mathbf{U}_{i-1}\mathbf{L}_{i-1}^T$, are available. The samples can be given by the following formular:

584
$$\mathbf{X}_k^a(t_{i-1}) = \bar{\mathbf{X}}^a(t_{i-1}) + \sqrt{r + 1}\mathbf{L}_{i-1}(\boldsymbol{\Omega}_{k,i-1}\mathbf{C}_{i-1})^T \quad (7).$$

585 For $1 \leq k \leq r + 1$, the \mathbf{C}_{i-1} is the Cholesky decomposition of \mathbf{U}_{i-1}^{-1} and $\boldsymbol{\Omega}_{i-1}$ is a $(r + 1) \times r$ ma-
586 trix with orthonormal columns and zero column sums, where $\boldsymbol{\Omega}_{k,i-1}$ denotes the k^{th} row of $\boldsymbol{\Omega}_{i-1}$. $\bar{\mathbf{X}}^a$
587 is the average of the analysis state.

588

589 **Acknowledgment**

590 The research presented in this study was funded by the Swedish Space Board within the project ‘As-

591 simulating SLA and SST in an operational ocean forecasting mode for the North Sea and Baltic Sea

592 using satellite observations and different methodologies’ (grant no.172/13). We thank Dr. Svetlana

593 Losa and one anonymous reviewer for their valuable comments that helped improve the manuscript.

594

595 **References**

596 Adcroft, A., and Campin, J. M.: Re-scaled height coordinates for accurate representation of free-

597 surface flows in ocean circulation model, *Ocean Modell.*, 7, 269–284, 2004.

598

599 Alenius, P. A., Nekrasov, A., and Myrberg, K.: Variability of the baroclinic Rossby radius in the Gulf

600 of Finland, *Cont. Shelf Res.*, 23 (6), 563–573, 2003.

601

602 Beckmann, A., and Döscher, R.: A method for improved representation of dense water spreading over

603 topography in geopotential-coordinate models, *J. Phys. Oceanogr.*, 27, 581–591, 1997.

604
605
606
607
608
609
610
611
612
613
614
615
616
617
618
619
620
621
622
623
624
625
626
627
628
629
630
631

Brisson, A., Le Borgne, P., and Marsouin, A.: Results of one year of preoperational production of sea surface temperatures from GOES-8, *J. Atmos. Oceanic Technol.*, 19(10), 1638–1652, 2002.

Dahlgren, P., Kållberg, P., Landelius, T. and Undén, P.,: EURO4M Project Report, D 2.9 Comparison of the Regional Reanalyses Products with Newly Developed and Existing State-of-the Art Systems. Technical Report, Online at: <http://www.euro4m.eu/Deliverables.htm>, 2014.

Donnelly, C., Andersson, J. C., and Arheimer, B.: Using flow signatures and catchment similarities to evaluate the E-HYPE multi-basin model across Europe, *Hydrological Sciences Journal*, 61, 255–273, 2016.

Egbert, G. D., and Erofeeva, S. Y.: Efficient inverse modeling of barotropic ocean tides, *J. Atmos. Oceanic Technol.*, 19(2), 183–204, doi: 10.1175/1520-0426, 2002.

Fennel, W., Seifert, T., and Kayser, B.: Rossby radii and phase speeds in the Baltic Sea. *Cont. Shelf Res.*, 11(1), 23–26, 1991.

Fu, W.W., She, J., and Dobrynin, M.: A 20-year reanalysis experiment in the Baltic Sea using three-dimensional variational (3DVAR) method. *Ocean Sci.*, 8, 827–844, 2012.

Galperin, B., Kantha, L. H., Hassid, S., and Rosati A.: A quasi-equilibrium turbulent energy model for geophysical flows, *J. Atmos. Sci.*, 45, 55–62, 1988.

Haines, K.: Ocean data assimilation. In: *Data Assimilation: Making Sense of Observations.* . Springer-Verlag, Berlin Heidelberg, pp. 517-548. ISBN 9783540747024, 2010.

Hordoir, R., Axell, L., Löptien, U., Dietze, H., and Kuznetsov, I.: Influence of sea level rise on the

632 dynamics of salt inflows in the Baltic Sea, *J. Geophys. Res. Oceans*, 120, doi:10.1002/2014JC010642,
633 2015.

634

635 Hordoir, R., Dieterich, C., Basu, C., Dietze, H., and Meier M.: Freshwater outflow of the Baltic Sea
636 and transport in the Norwegian current: A statistical correlation analysis based on a numerical experi-
637 ment, *Cont. Shelf Res.*, 64, 1–9, doi:10.1016/j.csr.2013.05.006, 2013.

638

639 Høyer J.L., and Karagali, I.: Sea Surface Temperature Climate Data Record for the North Sea and
640 Baltic Sea. *JOURNAL OF CLIMATE*. 29, 2529–2541, 2016.

641

642 Janjić, T., Nerger, L., Albertella, A., Schröter, J., Skachko, S.: On domain localization in ensemble
643 based Kalman filter algorithms. *Monthly Weather Review*, 136 (7), 2046–2060, 2011.

644

645 [Janjić, T. , Bormann, N. , Bocquet, M. , Carton, J. A., Cohn, S. E., Dance, S. L., Losa, S. N., Nichols,](#)
646 [N. K., Potthast, R. , Waller, J. A. and Weston, P.: On the representation error in data assimilation.](#)
647 [Q.J.R. Meteorol. Soc.. doi:10.1002/qj.3130, 2017.](#)

648

649 Kilpatrick, K. A., Podesta, G. P., and Evans, R.: Overview of the NOAA/NASA Advanced Very High
650 Resolution Radiometer Pathfinder algorithm for sea surface temperature and associated matchup data-
651 base, *J. Geophys. Res.*, 106(C5), 9179–9197, doi:10.1029/1999JC000065, 2001.

652

653 Large, W. G., and Yeager, S.: Diurnal to decadal global forcing for ocean and sea-ice models: The
654 data sets and flux climatologies, NCAR Tech. Note, NCAR/TN-4601STR, CGD Div. of the Natl.
655 Cent. for Atmos. Res., 2004.

656

657 Leclair, M., and Madec, G.: A conservative leapfrog time stepping method, *Ocean Modell.*, 30, 88–94,
658 doi:10.1016/j.ocemod.2009.06.006, 2009.

659

660 Leppäranta, M., and Myrberg, K.: The Physical Oceanography of the Baltic Sea, pp. 378, Springer-
661 Verlag, Berlin-Heidelberg, New York, 2009.

662

663 Levitus, S., and Boyer, T. P.: Salinity, in World Ocean Atlas 1994, NOAA Atlas NESDIS, vol. 3, 99
664 pp., U.S. Gov. Print. Off., Washington, D. C., 1994.

665

666 Liu, Y., Zhu, J., She, J., Zhuang, S. Y., Fu, W.W., and Gao, J.D.: Assimilating temperature and salini-
667 ty profile observations using an anisotropic recursive filter in a coastal ocean model. *Ocean Model.* 30,
668 75–87, 2009.

669

670 Liu, Y., Meier, H. E. M., and Axell, L.: Reanalyzing temperature and salinity on decadal time scales
671 using the ensemble optimal interpolation data assimilation method and a 3-D ocean circulation model
672 of the Baltic Sea. *J. Geophys. Res.Oceans.*, 118, 5536–5554, 2013.

673

674 Liu, Y., Meier, H. E. M., and Eilola, K.: Improving the multiannual, high-resolution modelling of bio-
675 geochemical cycles in the Baltic Sea by using data assimilation, *Tellus A*, 66, 24908,
676 doi:10.3402/tellusa.v66.24908, 2014.

677 Liu, Y., Meier, H. E. M., and Eilola, K.: Nutrient transports in the Baltic Sea – results from a 30-year
678 physical–biogeochemical reanalysis. *Biogeosciences*, 14, 2113–2131, 2017.

679

680 Losa S.N., Danilov, S., Schröter, J., Nerger, L., Maßmann, S., and Janssen, F.: Assimilating NOAA
681 SST data into the BSH operational circulation model for the North and Baltic Seas: Inference about
682 the data. *Journal of Marine Systems*, 105–108,152–162, 2012.

683

684 Losa S.N., Danilov, S., Schröter, J., Janjic, J., Nerger, L., and Janssen, F.: Assimilating NOAA SST
685 data into the BSH operational circulation model for the North and Baltic Seas: Part 2. Sensitivity of
686 the forecast's skill to the prior model error statistics. *Journal of Marine Systems*, 259–270, 2014.

687

688 Madec, G.: NEMO ocean engine, version 3.3, Note du Pôle de modélisation de l'Inst. Pierre-Simon
689 Laplace 27, Inst. Pierre-Simon Laplace, Paris. (Available at <http://www.nemo-ocean.eu/>), 2010.
690

691 Malanotte-Rizzoli, P, and Tziperman, E.: The oceanographic data assimilation problem: overview,
692 motivation and purposes. In *Modern Approaches to Data Assimilation in Ocean Modeling*, Amster-
693 dam: Elsevier, 3–17, 1996.
694

695 Nerger, L., Danilov, S., Hiller, W., and Schröter, J.: Using sea level data to constrain a finite-element
696 primitive-equation ocean model with a local SEIK filter. *Ocean Dynamics* 56, 634–649, 2006.
697

698 Nowicki, A., Dzierzbicka-Głowacka, L., Janecki, M., and Kałas, M.: Assimilation of the satellite SST
699 data in the 3D CEMBS model. *Oceanologia*, 57, 17–24, 2015.
700

701 O’Dea E. J., Arnold, A. K., Edwards, K. P., Furner, R., Hyder, P., Martin, M. J., Siddorn, J. R.,
702 Storkey, D., While, J., Holt, J. T., and Liu H.: An operational ocean forecast system incorporating
703 NEMO and SST data assimilation for the tidally driven European North-West shelf, *Journal of Opera-*
704 *tional oceanography*, 5(1), 3-17, 2012.
705

706 Oke, P. R., Schiller, A., Griffin, D. A., and Brassington, G. B.: Ensemble data assimilation for an ed-
707 dy-resolving ocean model of the Australian Region. *Q. J. Roy. Meteorol. Soc.* 131, 3301–3311, 2005.
708

709 Omstedt, A., Elken, J., Lehmann, A., Leppäranta, M., Meier, H.E.M., Myrberg, K., and Rutgersson,
710 A.: Progress in physical oceanography of the Baltic Sea during the 2003–2014 period. *Progress in*
711 *Oceanography*, 128, 139-171, 2014.
712

713 Pham, D.T.: Stochastic methods for sequential data assimilation in strongly nonlinear systems. *Mon.*
714 *Weather Rev.* 129, 1194–1207, 2001.
715

716 | [Pham, D. T., Verron, J. and M. C. Roubaud: A singular evolutive extended Kalman filter for data as-](#)
717 | [simation in oceanography. J. Mar. Syst.,16, 323–340, 1998.](#)
718 |
719 | Rodwell, M. J., Lang, S. T. K., Ingleby, N. B., Bormann, N., Hólm, E., Rabier, F., Richard-
720 | son, D. S., and Yamaguchi, M.: Reliability in ensemble data assimilation, *Q. J. Roy. Meteor. Soc.*,
721 | 142, 443–454, doi:10.1002/qj.2663, 2016.
722 |
723 | Samuelsson, P., Jones, C., Willen, U., Ullerstig, A., and co-authors.: The Rossby Centre Regional
724 | Climate model RCAS3: model description and performance, *TellusA*, 63, 4–23, 2011.
725 |
726 | She, J, Høyer, J. L., and Larsen, J.: Assessment of sea surface temperature observational networks in
727 | the Baltic Sea and North Sea. *Journal of Marine Systems* 65, 314–335, 2007.
728 |
729 | Stramska, M., and Białogrodzka, J.: Spatial and temporal variability of sea surface temperature in the
730 | Baltic Sea based on 32-years (1982—2013) of satellite data. *Oceanologia*, 57, 223–235, 2015.
731 |
732 | Tranchant B., Reffray, G., Greiner, E., Nugroho, D., Koch-Larrouy, A., and Gaspar, P.: Evaluation of
733 | an operational ocean model configuration at 1/12° spatial resolution for the Indonesian seas
734 | (NEMO2.3/INDO12) –Part 1: Ocean physics. *Geosci. Model Dev.*, 9, 1037–1064, 2016.
735 |
736 | Umlauf, L., and Burchard, H.: A generic length-scale equation for geophysical turbulence models, *J.*
737 | *Mar. Syst.*, 61, 235–265, 2003.
738 |
739 | Vancoppenolle, M., Fichefet, T., Goosse, H., Bouillon, S., Madec, G., and Maqueda, M. A. M.: Simu-
740 | lating the mass balance and salinity of arctic and Antarctic sea ice, *Ocean Modell.*, 27(1–2), 33–53,
741 | doi:10.1016/j.ocemod.2008.10.005, 2008.
742 |
743 | Väli, G., Meier, H. E. M., and Elken, J.: Simulated halocline variability in the Baltic Sea and its im-

744 pact on hypoxia during 1961–2007, *J. Geophys. Res.-Ocean.*, 118, 6982–7000,
745 doi:10.1002/2013JC009192, 2013.

746

747 Walton, C. C., Pichel, W. G., Sapper, F. J., and May, D. A.: The development and operational applica-
748 tion of nonlinear algorithms for the measurement of sea surface temperatures with NOAA polar-
749 orbiting environmental satellites, *J. Geophys. Res.*, 103(C12), 27,999–28,012,
750 doi:10.1029/98JC02370, 1998.

751

752

753

754

755

756

757

758

759

760

761

762

763

764

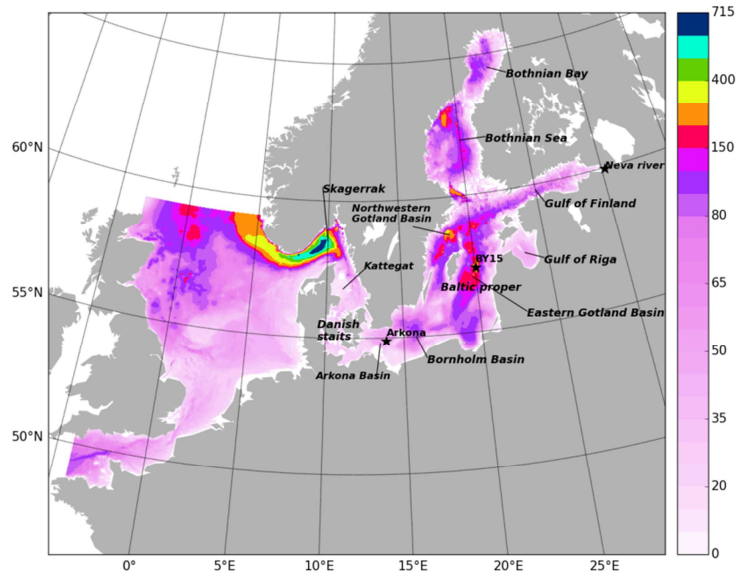
765

766

767

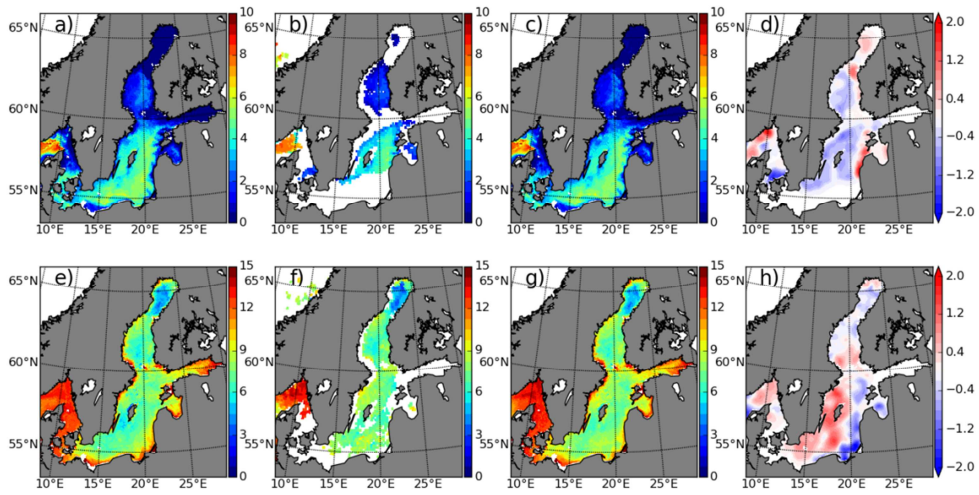
768

769



770
 771
 772
 773
 774
 775
 776
 777
 778
 779
 780
 781
 782
 783
 784
 785
 786
 787

Figure 1. Geographical domain and bathymetry (in m) of the NEMO-Nordic configuration.



788

789 Figure 2. Map of SST from FREE (a,e), OSISAF (b, f), ASSIM (c, g) and the assimilation increments

790 (d, h) on 11 January 2010 (first row) and 2 June 2010 (second row), respectively.

791

792

793

794

795

796

797

798

799

800

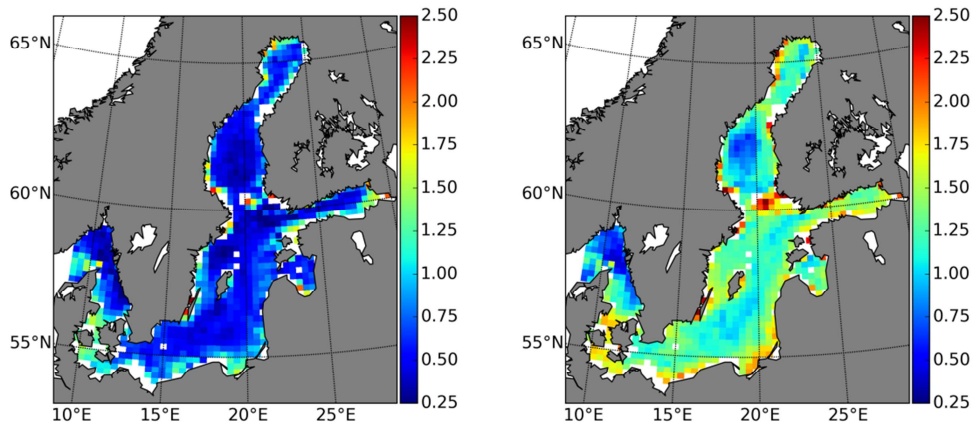
801

802

803

804

805



806

807 Figure 3. Map of the RMSE of SST from ASSIM (left panel) and FREE (right panel) calculated
808 against IceMap SST in 2010, respectively.

809

810

811

812

813

814

815

816

817

818

819

820

821

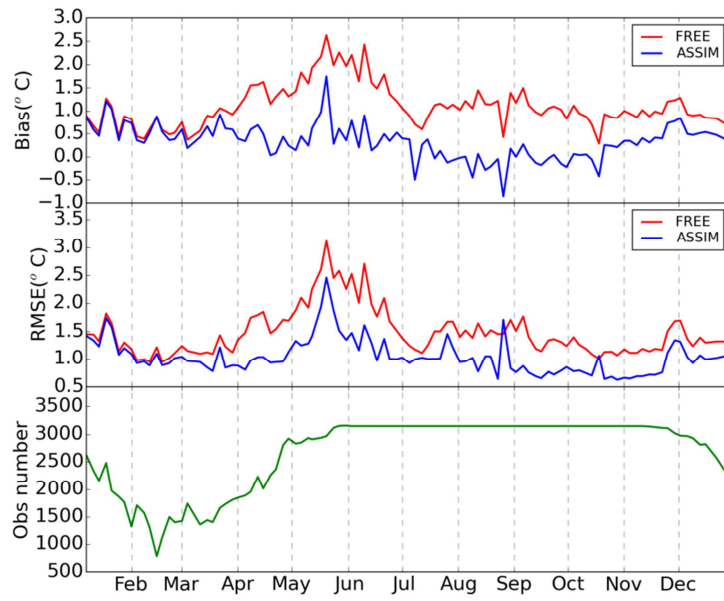
822

823

824

825

826



827

828 Figure 4. The evolution of basin-averaged bias and RMSE of SST from FREE and ASSIM relative to
 829 IceMap SST and the number of IceMap observation in 2010.

830

831

832

833

834

835

836

837

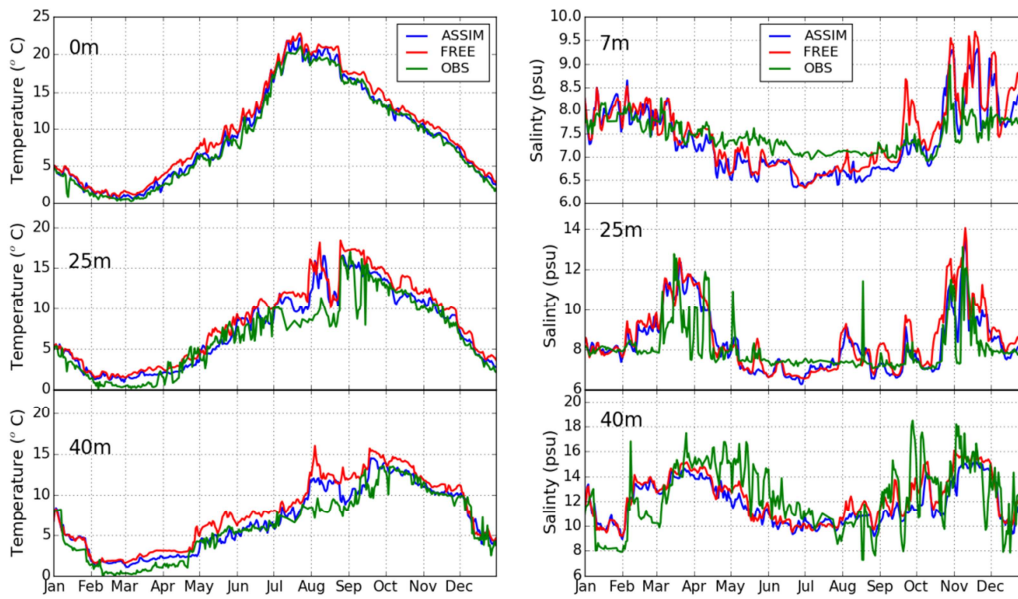
838

839

840

841

842



843

844 Figure 5. The time series of temperature (left panel) at a depth of 0, 25 and 40 m and salinity (right
 845 panel) at a depth of 7, 25 and 40 m at the Arkona station (13.87°E, 54.88°N), respectively.

846

847

848

849

850

851

852

853

854

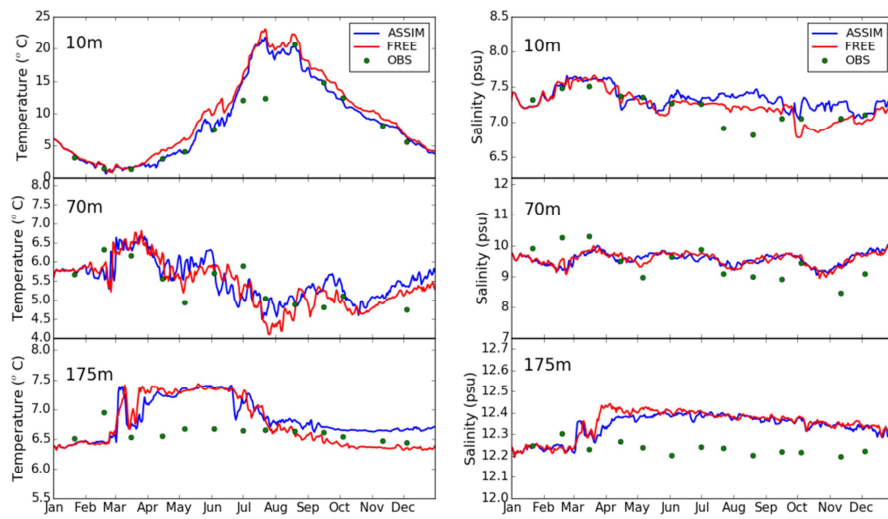
855

856

857

858

859



860

861 Figure 6. The time series of temperature (left panel) and salinity (right panel) at the BY15 station
 862 (20.05°E, 57.33°N) at a depth of 10, 70 and 175 m, respectively.

863

864

865

866

867

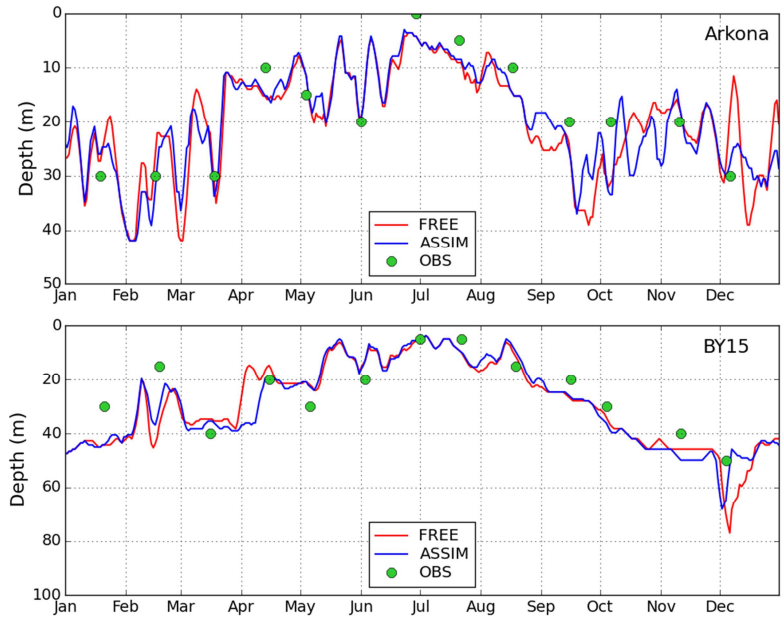
868

869

870

871

872



873

874 Figure 7. The time series of mixed layer depth at Arkona and BY15 station.

875

876

877

878

879

880

881

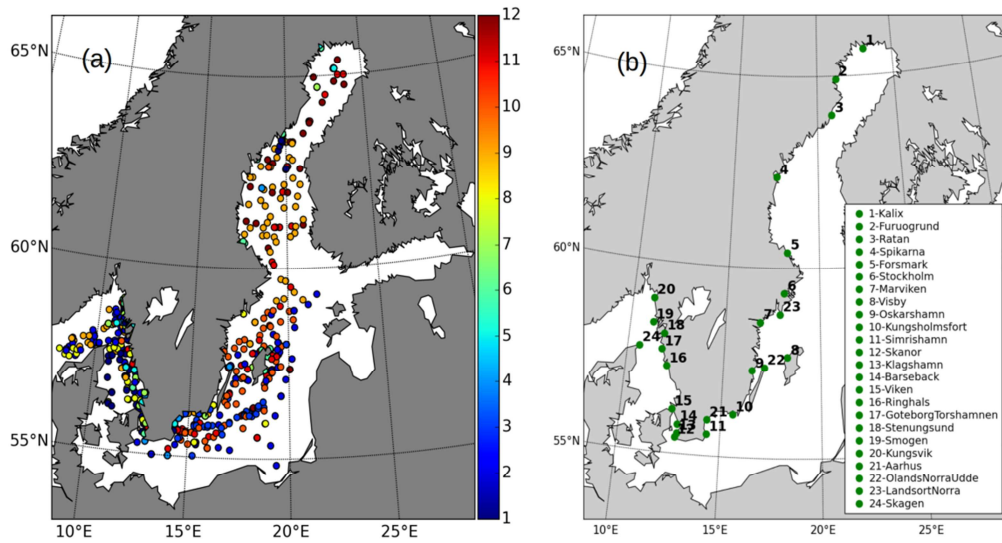
882

883

884

885

886



887

888 Figure 8. (a) Map of the temperature and salinity profiles from SHARK database in 2010. The colors
 889 show the observations months.(b) The tide gauges station along the Swedish coast.

890

891

892

893

894

895

896

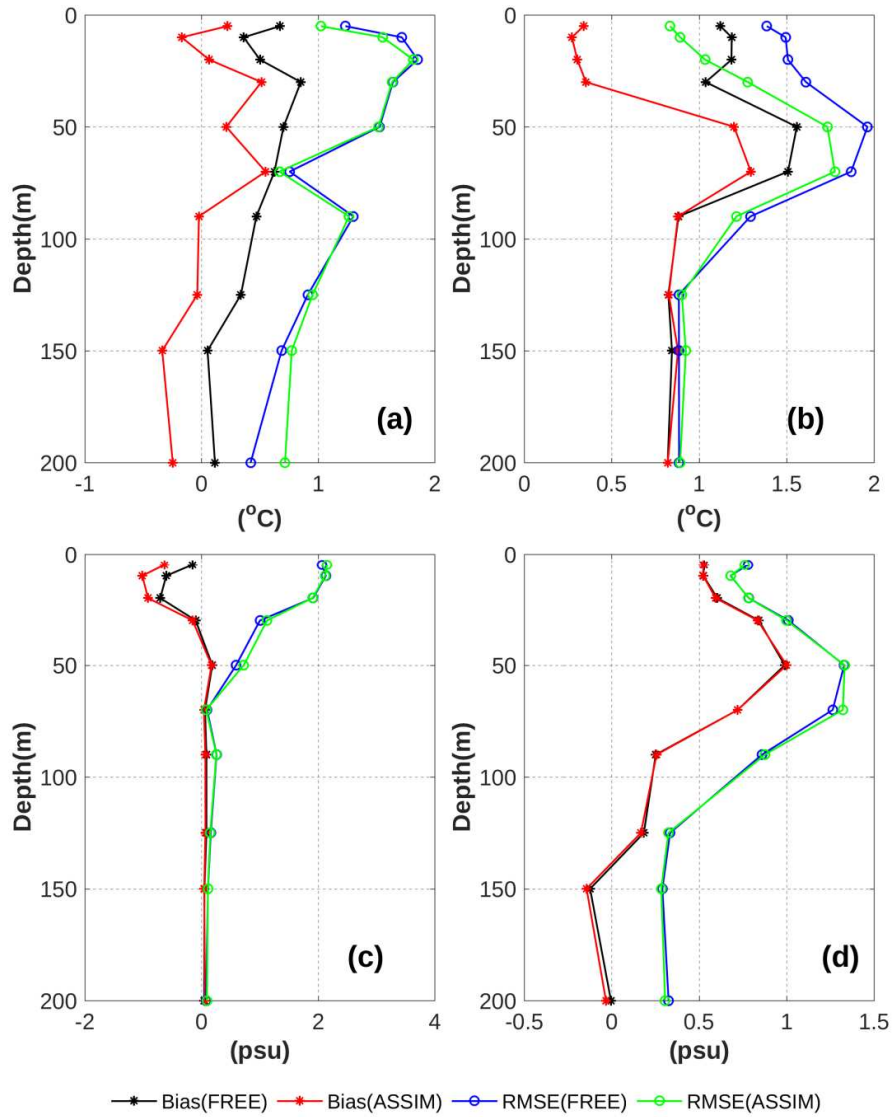
897

898

899

900

901



902

903 Figure 9. The overall RMSE and bias of temperature (up panel) and salinity (down panel) from FREE

904 and ASSIM relative to observations as a function of water depth inside (b,d) and outside (a,c) of the

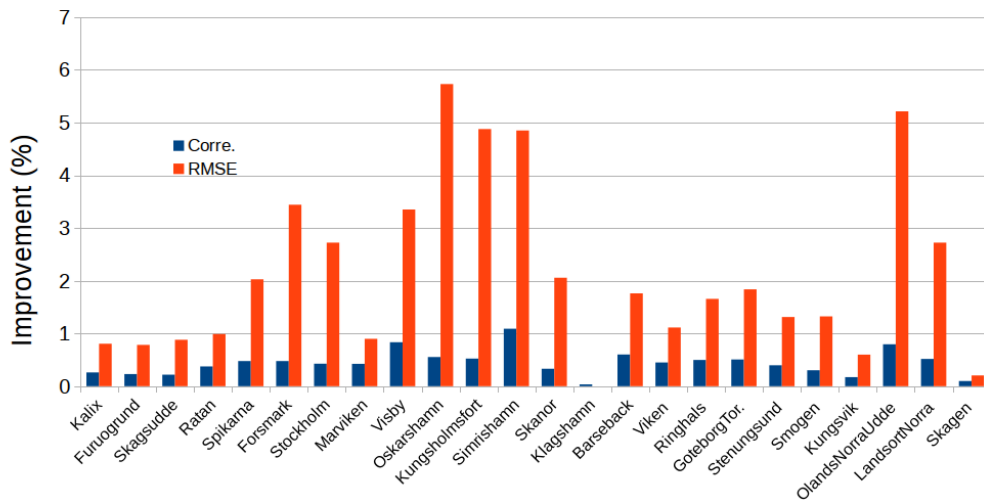
905 Baltic Sea.

906

907

908

909



910

911 Figure 10. The improvement (%) of correlation and RMSE for the SLA at the tide gauges stations. The
 912 station position is in the Figure 8b.

913

914

915

916

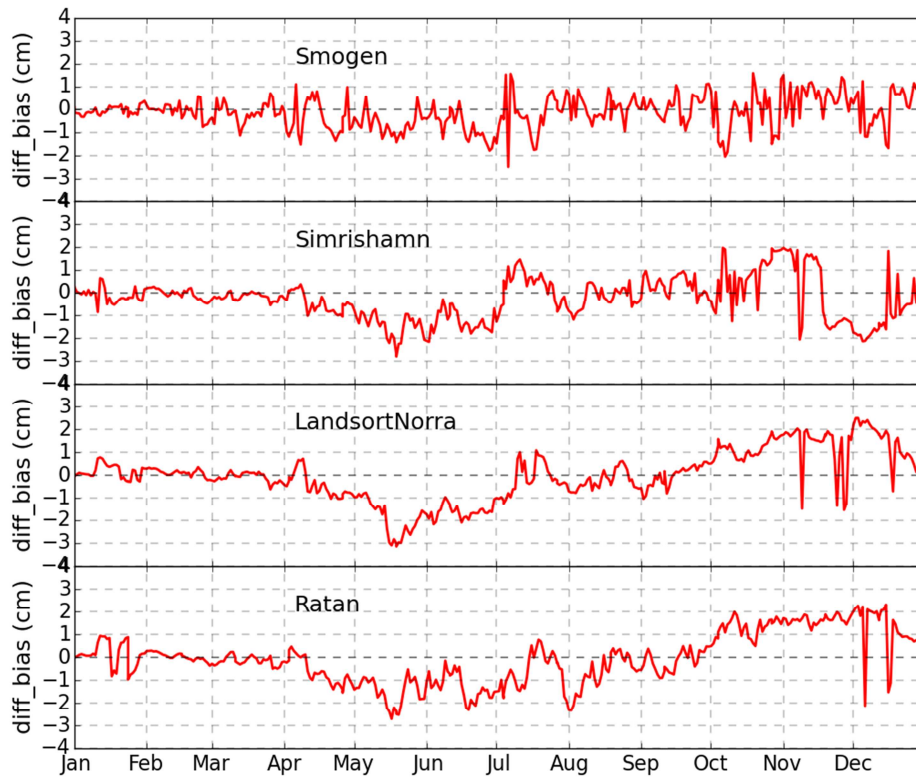
917

918

919

920

921



922

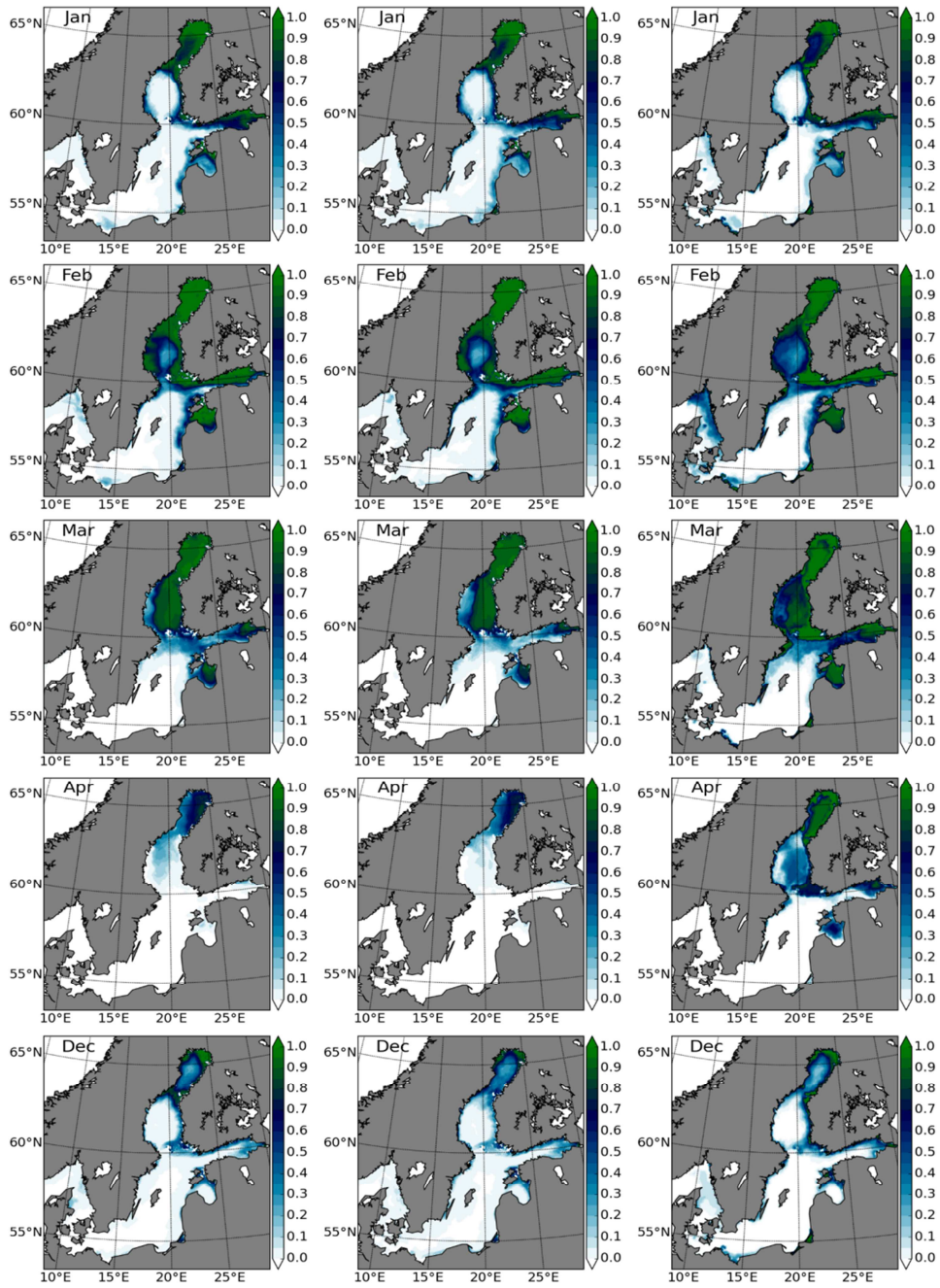
923 Figure 11. The variation of SLA biases in ASSIM relative to FREE against observations as a function
 924 of time. The station position is shown in the Figure 8b.

925

926

927

928



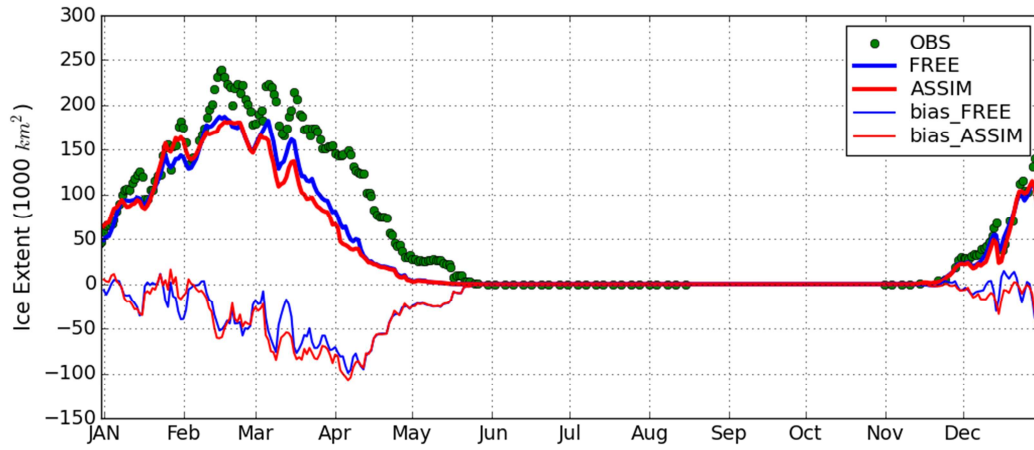
929

930 Figure 12. The monthly mean sea ice concentrations in FREE (left panel), ASSIM (middle panel) and
 931 IceMap (right panel), respectively.

932

933

934



935

936 Figure 13. The daily sea ice extent from FREE, ASSIM and IceMap and the sea ice extent bias (mod-
 937 elled minus observed field), respectively.

938